# Adhesion of Rhodium, Palladium, and Platinum to Alumina and the Reduction of NO on the Resulting Surfaces: A Theoretical Analysis

**Thomas R. Ward,† Pere Alemany,‡ and Roald Hoffmann***

*Department of Chemistry and Materials Science Center, Cornell University, Ithaca New York 14853-1301*

*Received: January 19, 1993*

We report here approximate molecular orbital computations of adhesion and NO reduction in the three-way catalyst, modeled by a monolayer of either Rh, Pd, or Pt on the (0001)O and (0001)Al faces of $\alpha$-$Al_2O_3$. The support is not electronically innocent but affects NO reduction capability significantly. Platinum and palladium form stable interfaces with both oxygen and aluminum faces. Only the aluminum interface is stable with rhodium. Depending on the nature of the interface, the Fermi level of the composite systems varies dramatically. This, in turn, affects the adsorption mode, molecular or dissociative, of nitric oxide. From our study, it appears that an oxygen–platinum interface is best suited for both dissociative adsorption of NO as well as the coupling of two adsorbed nitrosyls to form a reduced dinitrosyl species with significant N–N double-bond character.

## Introduction

The automobile is indispensible in our society. And it is also a major source of atmospheric pollution. The recent amendments to the US Clean Air Act set some stringent standards for the automotive industry.[1] To meet some of these by the end of the millenium will take much work, in which chemistry must participate. We believe that quantum mechanical modeling may aid in this effort.

Since 1981, rhodium has been a major component in automotive catalysts in order to meet the standards for $NO_x$ emissions.[2] Although the nitrosyl reduction mechanism has not been fully elucidated, it is generally accepted that nitrosyls adsorbed on group 9 metal surfaces[3–6] dissociate more readily than on group 10 ones.[7–13] This is often believed to be a key factor in determining the greater efficiency of Rh vs Pd or Pt in the nitrosyl reduction process in the three-way catalyst (TWC). In a previous paper, we examined NO reduction on *clean* Rh, Pd, and Pt surfaces and explained the special role of rhodium.[14]

Much of the experimental surface science work done on the interaction of NO with metals has been performed on well-defined single-crystal surfaces in high vacuum. For example, the interaction of NO with Al(100),[15] Si(100),[16] W(100) and -(110),[17] Re(001),[18] Ag(100) and -(111),[19,20] Mo(100) and -(111),[21] Pt(111),[8–10,20,22–25] Pd(100) and -(111),[11–13,26–28] and Rh(100) and -(111)[3,5,29,30] has been studied. Even for metals which do not traditionally form nitrosyl complexes, i.e., magnesium, silicon, aluminum, and silver, adsorbed NO species have been detected. Dissociative adsorption of NO to $N_2$ and $O_2$ has been observed on Ir, Mo, Al, Pt, Rh, Ru, Ni, Ti, and Zn.[8,31] In addition to linear $M(NO)^+$, bent $M(NO)^-$,[32–36] and atomic N and O adsorption, surface dinitrosyl species, $M(NO)_2$, have been reported on Pd-(100),[37] Pd(111),[26] and Pt(111) surfaces.[27,38]

The actual TWC systems consist of metals supported on oxides. Much experimental work has been done on Cr–$SiO_2$[39–42] as well as Ni–$SiO_2$.[43,44] In both cases dinitrosyl species, $M(NO)_2$, have been detected. Such dinitrosyl entities are also present with transition metals supported on alumina, e.g., Rh,[45,46] Cr, Mo, W,[47] and Co.[48,49] More recently, aluminosilicates (zeolites) have received increasing attention as supports. Again, dinitrosyl species recur in this field, i.e., Cr,[50] Co,[51,52] Fe,[53] and Rh[54,55] exchanged into X or Y zeolites, as well as $Cu^I$ exchanged into ZSM-5 zeolites.[56]

Many gas-phase reactions involving NO follow a third-order rate law, proportional to the square of the nitric oxide concentration. This is caused by the presence of a nitrosyl–dinitrogen dioxide preequilibrium.[57,58] Adsorbed dinitrosyl entities have received little attention as possible intermediates in the transition-metal-mediated reduction of nitric oxide. Their frequent occurrence, especially with supported catalysts, triggered our curiosity.

Adhesion of transition metals to oxide ceramics of course plays an important role in many industrial applications.[59,60] Recent studies in our group have been devoted to the adhesion of metals on $\alpha$-$Al_2O_3$[61,62] and on NiO.[63] Considering the composition of many industrial and automotive catalysts, we could not resist the temptation of merging our experience in both fields, surface adsorbate interaction and adhesion, applying that knowledge to model the TWC.

The most common TWC consists of a ceramic honeycomb whose composition is near that of pure corderite (2Mg, $2Al_2O_3$, $5SiO_2$), to which is applied the active catalyst. A typical composition of the latter can be ~14% $\gamma$-$Al_2O_3$, 1.6% NiO, 0.7% $CeO_2$, 0.15% Pt, and 0.015% Rh.[64] In this study, we focus on the supported precious metal, leaving for further investigation the role of both NiO and $CeO_2$.

## Goal

As we have shown in our previous contribution in the field,[14] the Fermi level of the metal surface determines the adsorption mode, molecular or dissociative, of the nitrosyl. The nature of the coupled product, whether it be dinitrogen dioxide or hyponitrite-like, depends as well on the Fermi level.

In the same spirit, we set out to analyze the role of the support in the platinum group metal-mediated NO reduction. We will first look at the characteristics of adhesion of Rh, Pd, and Pt on $Al_2O_3$. Then, nitric oxide will be adsorbed on the metal, and the effect of the metal–ceramic interface will be studied. Starting from these adsorption geometries, we examine a coupling path leading to $N_2O_2$. Both the adsorption mode of NO and the nature of the coupled product (whether it is a dinitrogen dioxide containing four $\pi$-electrons or a hyponitrite with six $\pi$-electrons) will be discussed as a function of the Fermi level of the catalyst.

## Adhesion

Let us review briefly the results of our earlier study of the interfaces formed between first-row transition metals and different

† Present address: ICMA, Université de Lausanne, Place du Château 3, CH-1005 Lausanne, Switzerland.
‡ Present address: Departament de Química Física, Universitat de Barcelona, Barcelona, Catalunya, Spain.

0022-3654/93/2097-7691$04.00/0 

faces of $\alpha$-$Al_2O_3$.[61,62] Two main interactions were found to dictate the strength and quality of adhesion:

(a) Net destabilizing O–M interactions (see **1**) are responsible for the weak (or even repulsive) adhesion energies found for oxide surfaces with high oxygen concentration. Filling of an interface M–O* band leads to a highly unfavorable situation in the case of high d-electron counts (late transition metals).

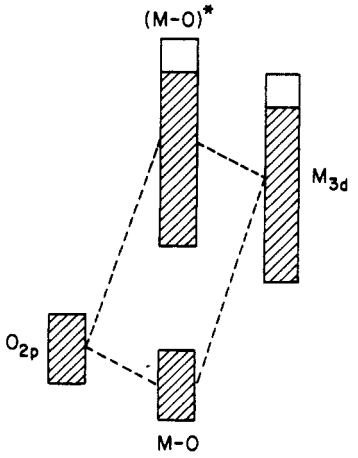


**1**

(b) Aluminum cations on the oxide surface are capable of forming strong charge-transfer bonds with the metal. These bonds result from interaction of empty aluminum dangling bond states with the d band of the metal **2**.

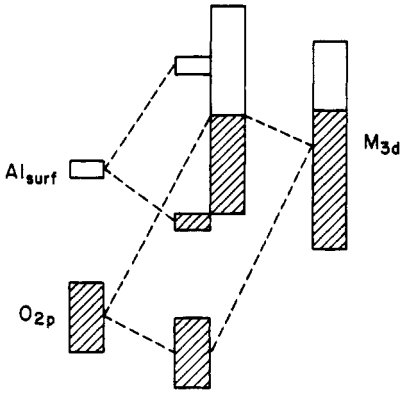


**2**

A balance of both interactions determines the adhesion of a particular transition metal to $\alpha$-$Al_2O_3$. The most important factor is the ratio of Al/O atoms directly exposed to the metal surface. Aluminum-rich surfaces are predicted to form strong interfaces with almost all first-transition-row metals, while oxygen-rich surfaces do not result in strong interfaces, especially with late transition metals. The coordination geometry of atoms at the surface does not seem to be a major factor in determining adhesion properties for different faces. For instance, calculations of the adhesion energy for first-row transition metals on different faces of $\alpha$-$Al_2O_3$ surfaces indicates that the (0001)O and the (0001)Al surfaces give upper and lower bounds for the adhesion energies. Surfaces with intermediate Al/O ratios yield interfaces with intermediate energies. These findings agree with recent experimental results by Ealet and Gillet for the alumina ($\bar{1}012$) surface.[65]

We will apply the extended Hückel tight-binding method[66–68] to analyze interface formation of Rh, Pd, and Pt on $\alpha$-$Al_2O_3$. Our attention will be focused on the changes induced in the metal slab by interaction with the alumina.

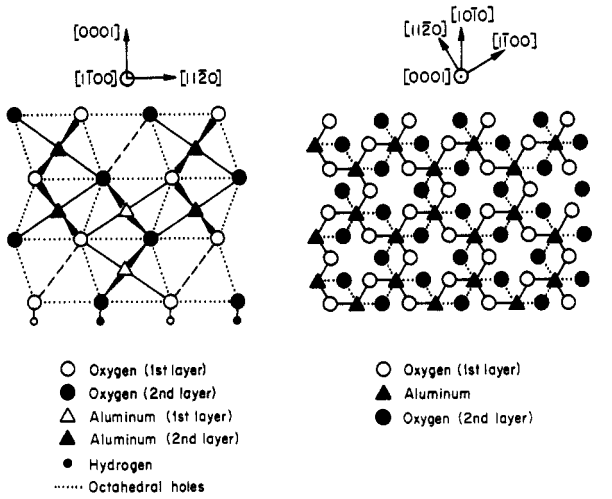


**Figure 1.** Top and side views of the (0001)O surface model slab of $\alpha$-$Al_2O_3$.

## Models

Our model of the interface consists of the superposition at a fixed distance (2.0 Å) of two two-dimensionally infinite slabs of oxide and metal. In our previous study,[61,62] the metal geometry was adjusted to fit the rigid $\alpha$-$Al_2O_3$ slab. Since our main purpose here is the comparison of NO and $N_2O_2$ adsorption on bare and supported metal catalysts, a different approach was followed. The transition metals were modeled by a slightly modified three-layer slab with the same geometry for all three metals. Rh, Pd, and Pt crystallize in the fcc structure with cell parameters 3.804, 3.891, and 3.924 Å, respectively.[69] In this study, we used the value of 3.803 Å for all three metal model slabs.[70] This value leads to a triangular (hexagonal close-packed) mesh with an M–M distance of 2.70 Å for each layer. The interlayer separation is 2.20 Å for the (111) face.

The oxide slab has been modified to provide epitaxy with the rigid metal slab. Our model consists of four layers of close-packed oxygen atoms with interlayer O–O distance of 2.70 Å. Three layers of aluminum cations, occupying two-thirds of the octahedral holes between oxygen layers, and a passivating hydrogen layer on the back surface of the slab, complete our model for the (0001)O face. In our model slab all aluminum atoms between two oxygen layers are located in a single plane, centering octahedral holes. All Al–O distances have the value 1.903 Å.

The (0001)Al face is modeled by a slab obtained by removal of both the topmost oxygen layer and one of the aluminum atoms on the first aluminum layer. Figure 1 shows a schematic representation of two views of the (0001)O surface model slab.

The validity of our idealization of the $\alpha$-$Al_2O_3$ structure is corroborated by the DOS plots obtained for both surfaces, which are in good agreement with our previous work and other studies, both experimental and theoretical.[61,62]

## Results

Table I shows the adhesion energy values obtained for both the (0001)O– and the (0001)Al–metal interfaces. For simplicity, we abbreviate these as $M_3$*on*O and $M_3$*on*Al, respectively. $M_3$ symbolizes a three layer metal slab. Surprisingly, we obtain stable interfaces for both Pd and Pt with the (0001)O surface, $Pd_3$*on*O and $Pt_3$*on*O. Such stabilization was not observed for Ni in our previous work.[61,62] The charge transfer, $\Delta q_M(e^-)$ (Table I), also indicates the magnitude of the charge transferred to the metal (positive values) or to the ceramic (negative values).

**TABLE I: Adhesion Energies and Charge Transfer for the (0001)O and the (0001)Al Metal Interfaces, $M_3onO$ and $M_3onAl$, Respectively**

| | $M_3onO$ | | | $M_3onAl$ | | | ionic contribution | |
|---|---|---|---|---|---|---|---|---|
| | eV/uc[a] | $J/m^2$ | $\Delta q_M(e^-)$[b] | eV/uc | $J/m^2$ | $\Delta q_M(e^-)$ | eV/uc | $J/m^2$ |
| Rh | 0.483 | 0.409 | +0.11 | -3.616 | -3.059 | -0.32 | -0.874 | -0.739 |
| Pd | -0.921 | -0.779 | +0.16 | -1.999 | -1.691 | +0.11 | -0.135 | -0.114 |
| Pt | -0.324 | -0.274 | +0.16 | -2.508 | -2.122 | -0.24 | 0.000 | 0.000 |

[a] uc refers to unit cell. [b] $\Delta q_M(e^-)$ refers to the charge transfer.

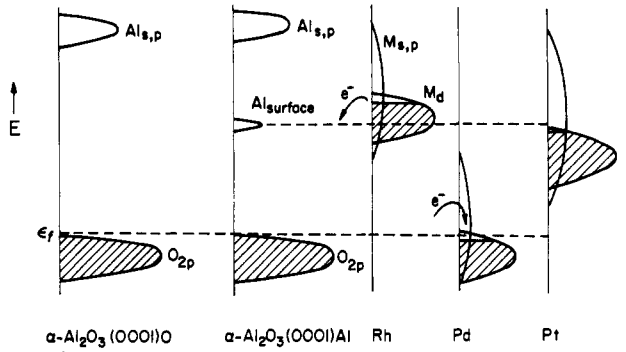


**Figure 2.** Qualitative illustration of charge transfer between metal and ceramic. The upper dashed line indicates the position of the Al surface states.

For the interaction with the aluminum surface a different factor, ionic charge transfer, has to be included in our discussion. This term arises from electrons transferred from the slab with the higher Fermi level to the other slab. It gives an additional stabilizing factor for the interface. In a one-electron calculation, such as the extended Hückel one we use, this ionic component is overestimated. To assess the relative magnitude of ionic charge transfer and covalent interactions, we performed two separate calculations with interfacial separations of 2.0 and 10.0 Å, respectively. At an interfacial distance of 10.0 Å all overlap terms between orbitals of both slabs, metal and ceramic, are zero, and the entire stabilization energy comes from the ionic term. The last entry of Table I shows that the magnitude of ionic charge transfer is important for Rh, moderate for Pd, and nonexistent for Pt. Analysis of the changes in average charge on the metal atoms leads to the qualitative diagram shown in Figure 2. From this figure we can see that the interface with Rh is unstable for the (0001)O surface, $Rh_3onO$, but strongly stabilized when interacting with the (0001)Al surface, $Rh_3onAl$. Important ionic charge transfer to the empty aluminum dangling states and the good energy match of these with the d band of the metal provide a substantial adhesion energy in this case.

The case of palladium, with stable interfaces for both $Pd_3onO$ and $Pd_3onAl$, is more complicated. Interaction of the d band with the O2p band gives a destabilizing contribution that is overcome by the attractive interaction of the empty metal s band with the O2p band of the oxide. The s band lies much lower for palladium than for rhodium and is able to interact much more (better energy match) with the oxide band. This mechanism of interface stabilization is corroborated by the electron transfer to the metal; almost all charge has been transferred to the s levels of palladium. The low-lying bands of palladium also give rise to an ionic charge transfer term, in an opposite direction in this case, electrons flowing from the oxide to the metal.

The interaction with platinum is intermediate between those of rhodium and palladium. The position of the Fermi level of the metal slab in this case does not permit any ionic charge transfer in either direction. For the (0001)O surface, $Pt_3onO$, a weak, attractive adhesion energy is found. The repulsive (O2p–Md) and attractive (O2p–Ms) interactions do not balance, and the latter dominates slightly. For the interface formed with the (0001)Al surface, $Pt_3onAl$, a good energy match of the metal d band with the dangling aluminum states provides better stabilization compared to palladium, $Pd_3onAl$. Compared to rhodium, however, the absence of ionic charge transfer and a poorer energy match results in a weaker interface.

**TABLE II: Summary of Fermi Level Variation (eV) as a Function of Interface and Metal**

| | $E_f$ ($M_3$) | $E_f$ ($M_3onO$) | $E_f$ ($M_3onAl$) | $E_f$ ($MonO$) | $E_f$ ($MonAl$) | $E_f$ ($M_2Al$) |
|---|---|---|---|---|---|---|
| Rh | -8.62 | -8.38 | -8.68 | -8.28 | -9.56 | -8.38 |
| Pd | -10.97 | -10.20 | -10.73 | -10.26 | -10.71 | -9.48 |
| Pt | -9.76 | -9.35 | -9.77 | -9.48 | -10.39 | -8.61 |

Our models of supported catalysts will consist of a single layer of metal atoms on both oxide surfaces, $MonO$, and aluminum surfaces, $MonAl$, respectively. It is thus important that all the trends, especially the change in the position of the Fermi level upon interaction, found for the three-layer slab models, be reproduced for these simpler cases. A comparison of both models (three layer vs one layer) shows good agreement in the basic features of the interaction. The changes observed for the Fermi levels agree in direction in all cases, although there is some variation in magnitude. The Fermi levels for all three metals, M = Rh, Pd, Pt, and interfaces are presented in Table II.

A model with metal coverage of 0.667 ML (ML = monolayer), where the transition-metal atoms sit in the empty aluminum positions of the surface, has also been considered. In this case, a mixed Al/M layer, abbreviated $M_2Al$ (**3**, M = Rh, Pd, Pt), is exposed to the adsorbate. The Fermi level for all three metals rises in this situation, compared to the bare metal slabs (Table II).

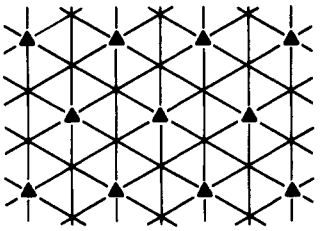

▲ Aluminum
✳ M (Rh, Pd, Pt)
$M_2Al$

**3**

## Real and Model Catalysts

It is important at this point to address briefly the similarities and differences between real supported catalysts and our models. Industrial catalysts use $\gamma$-$Al_2O_3$ as support because of the higher surface area of this material. Structural differences between $\alpha$-$Al_2O_3$ and $\gamma$-$Al_2O_3$ are important:[71] $\alpha$-$Al_2O_3$ has the corundum structure with all aluminum atoms occupying two thirds of the octahedral holes between oxygen layers, while $\gamma$-$Al_2O_3$ crystallizes in a vacant spinel structure in which there are only 21 and $^1/_3$ metal atoms arranged at random in the 16 octahedral and 8 tetrahedral positions of that structure. One important difference is the coexistence in the structure of $\gamma$-$Al_2O_3$ of tetrahedrally and octahedrally coordinated $Al^{3+}$ cations.

From our previous experience, the characteristics of adhesion are not strongly affected by the coordination geometry of the surface aluminum atoms.[61,62] The most important factor is the surface Al/O ratio for each face. Thus, it seems reasonable to assume that adhesion strength on the (0001)O and the (0001)Al faces of $\alpha$-$Al_2O_3$ will give lower and upper bounds for the adhesion of transition metals to different forms of alumina. The main features of the DOS for $\gamma$-$Al_2O_3$ will closely resemble those of $\alpha$-$Al_2O_3$; only the magnitude of the interaction of surface states with the metal bands may differ.

In the TWC the choice of $\gamma$-$Al_2O_3$ as a support is due to a great extent to its high surface area. This allows a high dispersion of the precious metal. In our models, we must assume coverages of 1 ML (*Mon*O and *Mon*Al) or $^2/_3$ ML ($M_2$Al), while in industrial catalysts the metal coverage used is never higher than 0.1 ML. The particle size of the noble metal rafts in a fresh TWC is less than 50 Å. This can increase to 1000 Å, or more, at the high temperatures of vehicle operation. Since most of the catalytic activity is preserved,[64] we may consider our metal coverage of 1.0 ML as approximating such large rafts. However, we cannot simulate interactions between the adsorbates and the support. The formation of rafts or islands thicker than one layer is also not incorporated in our models. This phenomenon can lead to adsorption of NO on a different face of the metal or to simultaneous interactions of the adsorbate with metal and support.

Computational constraints prevent us from using the $\gamma$-$Al_2O_3$ modification as the support. It should be pointed out, however, that $\alpha$-$Al_2O_3$, which has a considerably smaller unit cell, has been shown to be usable as the support in the TWC.[72,73]

Other effects that have been omitted in our models are modifications of metal–support interactions due to dopants in the oxide phase (NiO, $CeO_2$). Nickel oxide is added to the system to inhibit the diffusion of the precious metal in the spinel.[64] Cerium oxide is added to prevent sintering of the catalyst and to increase the dispersion of the noble metal.[74] Finally, physical characteristics of the support (polycrystalline, rough surfaces, diffusion of metal into oxide and of Al or O into the metal) were not included in our simulations either.

Despite our simplified model of a supported catalyst, we think that interesting conclusions can be extracted. Our hope is that these results will aid in the development of more elaborate models, that will in turn be able to give results of direct applied interest.

### The Adsorbate Comes into Action

As shown above, the supposedly inert support affects dramatically the Fermi level of the metal ceramic–composite system. Let us now study the consequence of this on the adsorption of both NO and $N_2O_2$.

The extended Hückel method does not allow reliable optimization of interatomic distances, so we must fix these. It is necessary to keep distances constant, so as to obtain a relative ordering of bond strengths for the systems considered. With this in mind, we set the N–O distance to 1.17 Å and the M–N distance to 1.8 Å for all calculations.

Since the coupling of two adsorbed nitrosyls will be considered, yielding dinitrogen dioxide, we include two NO's per unit cell. This simplifies the analysis, since both reactant **4** and coupled product **5** have the same number of FMO's. We shall focus on the interaction of the frontier orbitals of the adsorbate with the surface. For the adsorbate's FMO's, we introduce labels which hint at their origin, derived from $5\sigma$ and $2\pi$.

In the starting geometry, both nitrosyls lie parallel to each other, 2.70 Å apart. At this separation, the in- and out-of-phase linear combinations of the FMO's show practically no splitting. Bringing the two nitrosyls together in the *yz* plane, as depicted below, lifts the degeneracy of the $\pi_x$ and $\pi_y$ orbitals. As the nitrogens approach, the FMO's with N–N bonding character are stabilized, and the splitting between the in- and out-of-phase

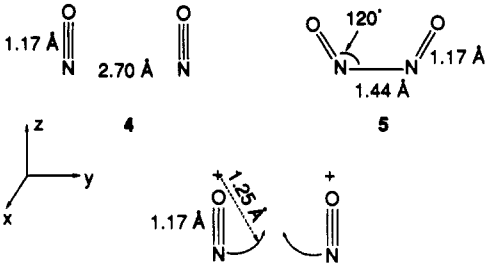


combinations becomes substantial. In **5**, the N–N distance was set to 1.44 Å.[14] A Walsh diagram for the coupling of two NO molecules with the formation of an N–N bond is presented in Figure 3.

Before considering specific adsorption geometries for both **4** and **5**, let us compare the molecular orbital energies of the adsorbates to the DOS of the metal slabs. Figure 4 depicts the DOS of the three three-layer slabs $Rh_3$, $Pd_3$, and $Pt_3$, as well as the MO levels for a nitrosyl and those of a dinitrogen dioxide **5**. Clearly, the bandwidths differ significantly from slab to slab, rhodium having the widest d band.

In our previous contribution, we showed that for nitrosyl chemisorption the energy term $E^\circ_i - E^\circ_j$ in the second-order perturbation, expression 1 dominates.[14] Independent of adsorption geometry, we found that the energy match controls the stabilization energy.

$$\Delta E = |H_{ij}|^2/(E^\circ_i - E^\circ_j) \qquad (1)$$

For a nitrosyl molecule, the $2\pi^*$ level is occupied by one electron. The computed N–O overlap population for a pair of nitrosyls **4** is 1.13. Upon interaction with a surface, if this level is located above the Fermi level, electrons will be dumped from the $2\pi^*$ level into the slab, resulting in strengthening of the N–O bond (Figure 5a). If the $2\pi^*$ level is located below the Fermi level, the electron flow is reversed, weakening the N–O bond (Figure 5b). This latter situation corresponds to backbonding in the Blyholder model, the bonding being provided to a great extent by the $5\sigma \rightarrow$ metal interaction.[75]

If the Fermi level of the metal slab is raised upon interaction with the ceramic, the electron flow may be reversed in the slab–adsorbate interaction. This will weaken the N–O bond, as $2\pi^*$ levels get populated. We shall next test this hypothesis with various interfaces and adsorption geometries of both nitrosyls **4** and dinitrogen dioxide **5**.

Since we are modeling the M(111) face of the metals, there are three common adsorption geometries of a linear nitrosyl adsorbate; *on-top* M(NO) **6a**, *bridging* M(NO) **6b**, and *capping* M(NO) **6c**. However, we must bear in mind that we need two nitrosyls in close proximity in order to couple them. The various adsorption geometries of linear M(NO) are depicted below:

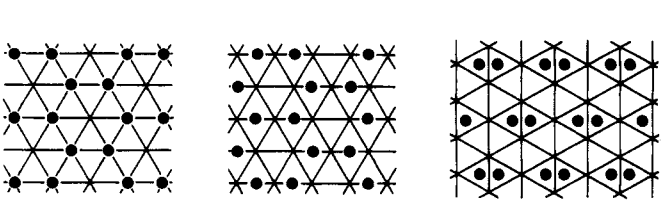


**6a** **6b** **6c**

In the *capping* M(NO) **6c** situation, two adjacent 3-fold hollows (over which are located the linear capping nitrosyls) are separated by only 1.56 Å for a metal-metal distance of 2.70 Å. At this

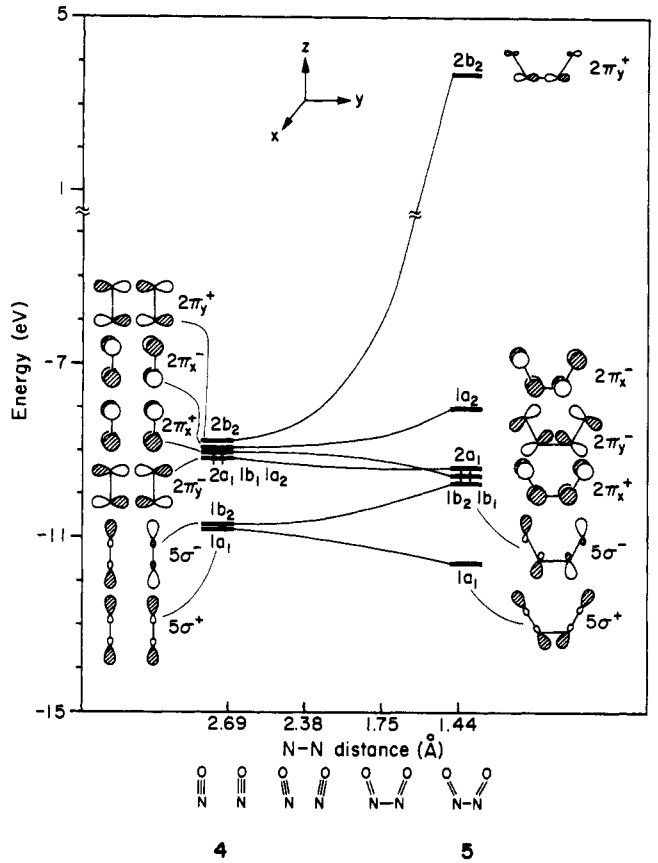


**Figure 3.** Walsh diagram for the coupling of a pair of nitrosyls **4** forming an N–N bond.

short separation, there is a strong oxygen–oxygen repulsion, which makes this geometry energetically unfavorable.

From these starting geometries, we may consider a number of coupling paths to afford adsorbed $N_2O_2$ **5**. Three of these are depicted below:

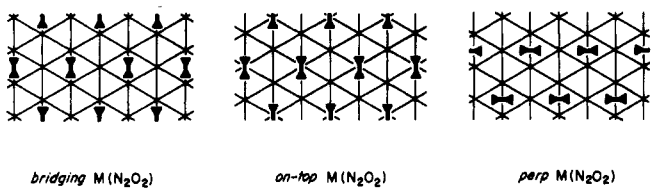


**7a** **7b** **7c**

We carried out a series of calculations of the three metal slabs with a metal oxygen interface, M*on*O, a metal aluminum interface, M*on*Al, and the mixed Al/M layer, $M_2Al$. Although there is experimental evidence for dissociative chemisorption of NO on Al(100) surfaces,[15] we will concentrate on the interaction of both NO **4** and $N_2O_2$ **5** with Rh, Pd, and Pt, rather than with either the oxide layer or the aluminum layer.

We shall discuss in detail the *on-top* M(NO) **6a** geometry and then review the other adsorption geometries, *bridging* M(NO) **6b** and *capping* M(NO) **6c**, keeping in mind that the energy term in (1), which is independent of adsorption geometry, dominates. Therefore, similar results are expected for these geometries.

### *On-Top* M(NO) 6a

In Figure 6a, we plot the Fermi levels for the *on-top* M(NO) **6a** geometry with M = Rh, Pd, and Pt. Along the abscissa we report the various metal-support interactions for $M_3$, the bare metal three-layer slab, a one-layer slab over an oxygen layer, M*on*O, a one-layer slab over an aluminum surface, M*on*Al, and the mixed layer slab, $M_2Al$. The dotted line marks the energy level of the $2\pi^*$ orbital of a pair of nitrosyls **4**. From this figure alone, *we conclude that the ceramic support significantly affects the Fermi level of the composite system.* As discussed in the adhesion section, changing the nature of the support from aluminum M*on*Al, to oxygen, M*on*O and $M_2Al$, drastically perturbs the Fermi level and consequently the electron flow between adsorbate and slab. Clearly, the rhodium slab stands out, with its Fermi level consistently above the $2\pi^*$ level. For all slabs, the metal on the mixed layer $M_2Al$ gives rise to the highest Fermi levels. In fact, the *on-top* $Pt_2Al(NO)$ situation ($E_f$ = –8.25 eV) has a higher Fermi level than both the bare rhodium slab, *on-top* $Rh_3(NO)$ ($E_f$ = –8.45 eV) and *on-top* Rh*on*Al(NO) ($E_f$ = –8.59 eV).

Let us trace down the substrate–catalyst interactions by using a crystal orbital overlap population (COOP) analysis.[76] The COOP curves for all four *on-top* Pt(NO), situations, $Pt_3$, Pt*on*O, Pt*on*Al, and $AlPt_2$ are depicted in Figure 7a–d, respectively. In the *on-top* $Pt_3(NO)$ case, the Fermi level ($E_f$ = –9.21 eV) lies below the $2\pi^*$ levels, which are mostly concentrated between –9.0 and –8.2 eV. The computed N–O overlap population is 1.23, greater than that of a pair of nitrosyls **4** (1.13, Figure 7a). When the ceramic–metal composite interacts via an oxygen contact, Pt*on*O, the Fermi level rises to –8.82 eV. As the Fermi level reaches the bottom of the $2\pi^*$ levels, the electron flow is reversed and the resulting N–O overlap population is significantly reduced (0.88, Figure 7b). The Fermi level sinks below the $2\pi^*$ levels for the Pt*on*Al situation, and the N–O overlap population consequently rises to 1.25 (Figure 7c). In the $Pt_2Al$ case, the Fermi level penetrates well into the $2\pi^*$ levels of the adsorbate **4**; these levels pick up bandwidth. The resulting N–O overlap population is computed at 0.80 (Figure 7d). In this case the interaction between the slab and the adsorbate $2\pi^*$ levels is strong. The presence of levels between –10.5 and –8.5 eV corresponds to the bottom of the $2\pi^*$-metal band. These levels are M–N bonding and N–O antibonding, as reflected in the respective COOP curves (not shown here).

Let's consider the results presented in Figure 6b. We report here the N–O overlap population as a function of metal slab and all four adhesion situations. The horizontal line corresponds to the N–O overlap population for a pair of nitrosyls **4** (1.13). From our computations, it appears the interaction between both $5\sigma^+$ and $5\sigma^-$ levels and the slab is more or less independent of the nature of the latter. Comparing both $5\sigma$ electron occupations after interaction for all metal and interface situations, we see that these numbers vary little. Of the two electrons present before interaction, ~0.25 electrons are donated to the slab. (The actual values range from 0.31 to 0.22 electrons donated). Therefore, we can expect the N–O overlap population to correlate closely with the Fermi level. This is nicely reflected in the comparison the Fermi level for various slabs and adhesion situations in Figure 6a with the corresponding N–O overlap population (Figure 6b). As the Fermi level rises above the $2\pi^*$ level, the N–O overlap population drops below that of free N–O (1.13), indicative of bond weakening in the adsorbate. For all three slabs, this effect is most dramatic for the $M_2Al$ situation.

### Other Adsorption Geometries of M(NO)

The trends reported for *on-top* M(NO) **6a**, Figure 6, are also present in the *bridging* M(NO), **6b**, case. Both Fermi level and N–O overlap population are summarized graphically in Figure 8a,b respectively. We will not discuss here the site preference for linear NO. Contributions from this group examined this for both Ni(111)[77] as well as Rh(100).[78]

In this absorption geometry, the Fermi levels of the supported catalysts are shifted up more in energy than in *on-top* M(NO) **6a**, resulting in smaller N–O overlap populations. It seems that *bridging* M(NO) **6b** should be more prone to cleave NO into its atomic components.

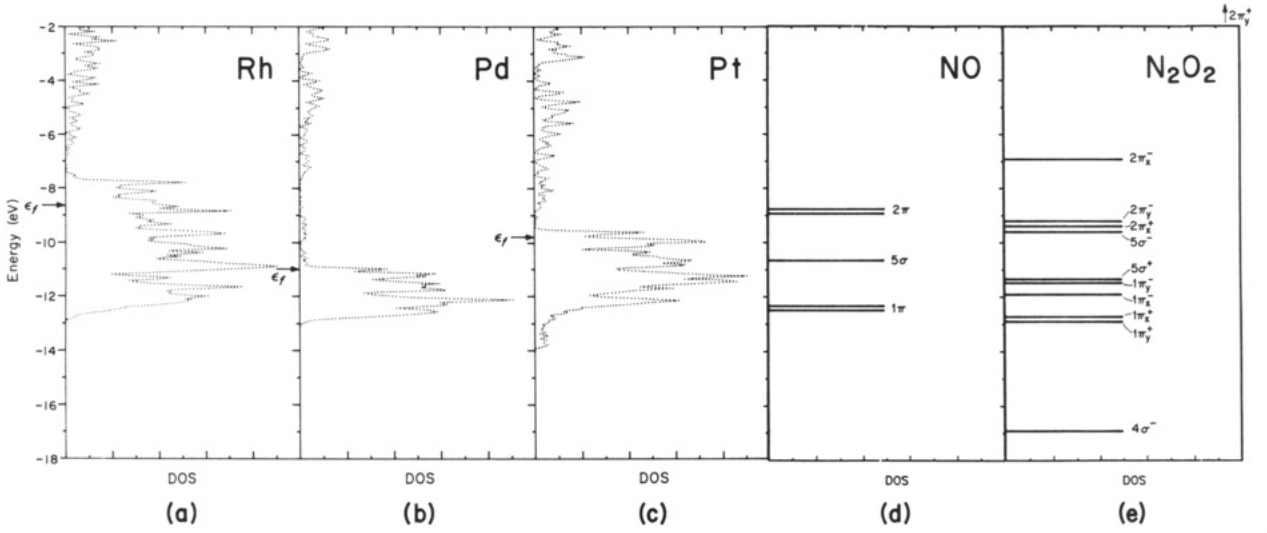


**Figure 4.** (a–c) Total DOS of a three layer metal slab $M_3$ where (a) M = Rh, (b) M = Pd, (c) M = Pt, (d) MO levels of NO, (e) MO levels of $N_2O_2$ **5**.

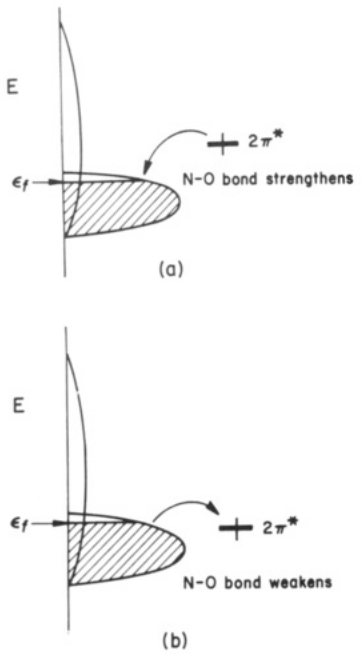


**Figure 5.** Effect of Fermi level on the N–O Bond strength.

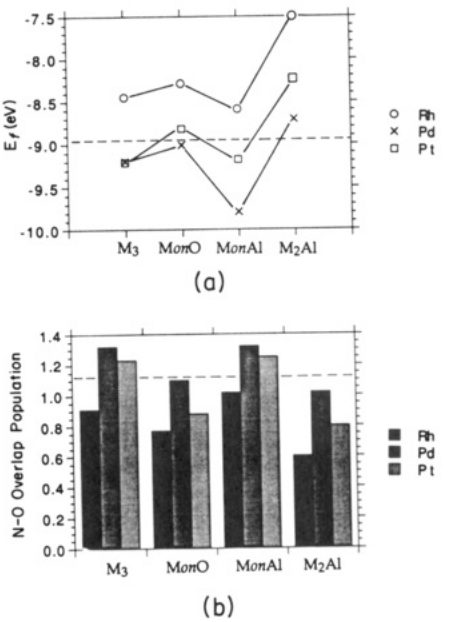


**Figure 6.** (a) Fermi level variation for *on-top* M(NO) and (b) resulting N–O overlap population. The horizontal line in (a) corresponds to the $2\pi^*$ energy of nitrosyl and (b) corresponds to the N–O overlap population a pair of nitroysls **4**.

Turning to *capping* M(NO) **6c**, we are faced with a problem due to the very large adsorbate–adsorbate repulsion. Rather than presenting results for this unrealistic adsorption geometry, we show in Figure 9 what happens at a coverage of 0.33ML.

Surprisingly, here the Fermi level of *capping* Rh*on*Al(NO) drops below that of both Pd and Pt analogs. However, for all metal–ceramic interfaces, the N–O overlap population is smallest with rhodium as catalyst.

From the results presented here, it appears that the supporting ceramic plays an active role in determining the adsorption mode of NO on supported catalysts. A metal–oxygen interface raises the Fermi level, eventually favoring dissociative adsorption of NO. In the adhesion section, however, we concluded that only palladium and platinum could form stable interfaces with oxygen as well as with aluminum. For all adsorption geometries, Pt*on*O(NO) is competitive with Rh*o*NAl (the only stable rhodium–ceramic interface) for the dissociative adsorption of NO.

## $N_2O_2$

We turn to the coupled product dinitrogen dioxide **5**. At this stage, we shall not only focus our attention on the N–O overlap population, but also on the N–N overlap population. We wish to form an intermediate $N_2O_2$ **5**, with a strong N–N bond and a weak N–O bond—product like, $N_2 + O_2$, in the sense of the Hammond postulate.

For this purpose, it is worthwhile to consider briefly the molecular orbitals of dinitrogen dioxide **5** (Figure 3). The orbitals derived from $5\sigma$, mostly lone pairs, contribute to some extent to N–O bonding. The in-phase combination $5\sigma^+$ is N–N bonding while the out-of-phase MO is weakly N–N antibonding. All $2\pi^*$ orbitals have N–O antibonding character. However, only the two lowest ones, $2\pi_x^+$ (the HOMO, –9.54 eV) and $2\pi_y^-$ (the LUMO, –9.37 eV), are N–N bonding. Significantly populating both these orbitals upon interaction with a slab contributes to a strong N–N bond, eventually leading to a reduced species containing an N–N double bond and a $6\pi$-electron system: hyponitrite **8**.

However, as the Fermi level rises further, the $2\pi_x^-$ orbital, at –7.97 eV, can interact and gets populated. This weakens the N–N bond, as this orbital is both N–N and N–O antibonding. Finally, the $2\pi_y^+$, at 3.68 eV, is off-scale for any interaction with a metal slab and does not get populated.

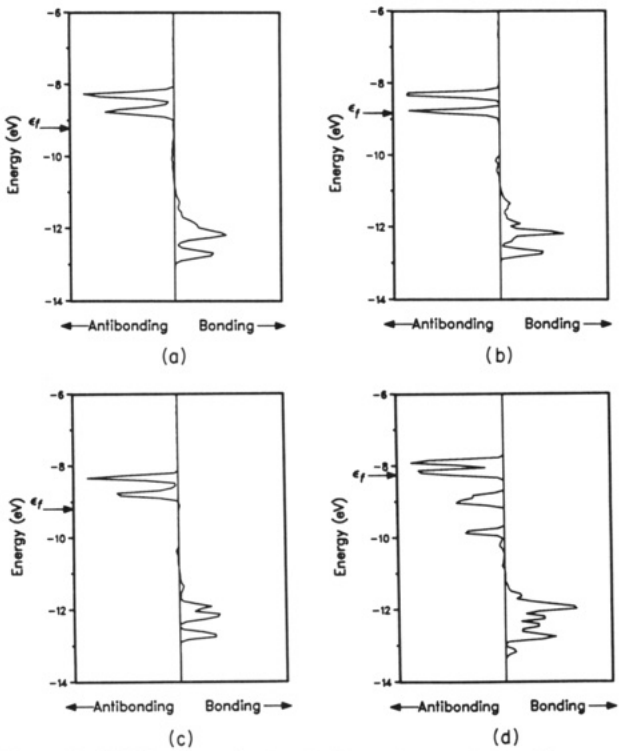


**Figure 7.** COOP curves for the N–O overlap population (a) *on-top* $Pt_3(NO)$ (1.23); (b) *on-top* Pt*on*O(NO) (0.88); (c) *on-top* Pt*on*Al(NO) (1.25), and (d) *on-top* $Pt_2Al(NO)$ (0.80).

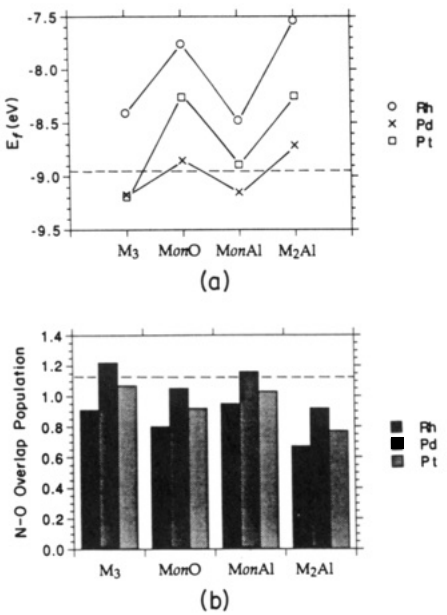


**Figure 8.** (a) Fermi level variation for *bridging* M(NO) **6b** and (b) resulting N–O overlap population. The horizontal line in (a) corresponds to the $2\pi^*$ level of NO and (b) corresponds to the N–O overlap population a pair of nitrosyls **4**.

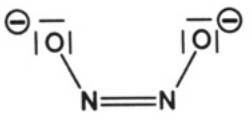

**8**

### *Bridging* $M(N_2O_2)$ 7a

From *on-top* M(NO) **6a**, a nitrosyl–nitrosyl coupling most naturally leads to *bridging* $M(N_2O_2)$ **7a**. The Fermi level, as well as N–O and N–N overlap populations, are presented in Figure 10a–c, respectively.

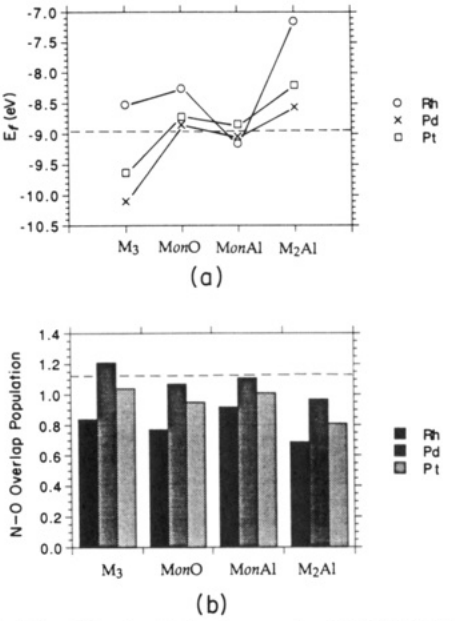


**Figure 9.** (a) Fermi level variation for *capping* M(NO) (0.33 ML) and (b) resulting N–O overlap population. The horizontal line in (a) corresponds to the $2\pi^*$ level of NO and (b) corresponds to the N–O overlap population of NO.

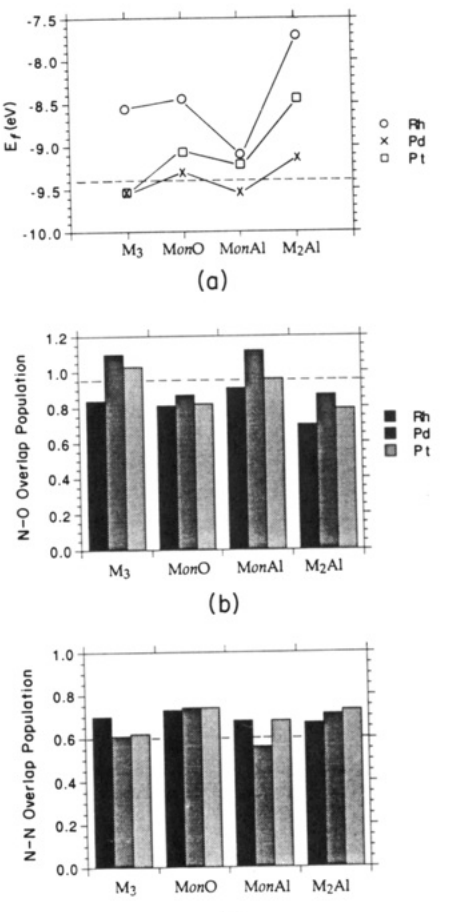


**Figure 10.** (a) Fermi level variation for *bridging* $M(N_2O_2)$ **7a**; (b) resulting N–O overlap population and (c) resulting N–N overlap population. The horizontal line corresponds to (a) the $2\pi_y^-$ level of $N_2O_2$; (b) the N–O overlap population of $N_2O_2$ **5** and (c) the N–N overlap population of $N_2O_2$ **5**.

Here again, the rhodium Fermi levels are consistently highest and the corresponding N–O overlap population smallest. As the Fermi level rises, e.g. *bridging* Rh*on*O$(N_2O_2)$ and *bridging* $Rh_2Al(N_2O_2)$, the $2\pi_y^-$ FMO gets populated. This is reflected

by a decrease in the N–N overlap population (Figure 10c). It is therefore no surprise to see the N–N overlap population of both *bridging* $Rh_2$*on*$O(N_2O_2)$ (0.73) and *bridging* $Rh_2Al(N_2O_2)$ (0.67) smaller than those of either palladium or platinum analogs.

We also examined the computed reaction enthalpy of *on-top* M(NO) **6a** → *bridging* $M(N_2O_2)$ **7a** as a function of metal and interface. The detailed results are not presented here, but reaction intermediate **5** seems energetically accessible in most cases. Consistently, the smallest reaction enthalpies are encountered with platinum as a catalyst, and/or metal oxide interfaces. The extended Hückel calculations predict the reaction *on-top* Pt*on*O(NO) → *bridging* Pt*on*$O(N_2O_2)$ to be thermoneutral. However, we do not trust these calculations in their quantitative detail; especially the energetics, a weak point of extended Hückel calculations. If we look at the bonding in the *on-top* Pt*on*O(NO) → *bridging* Pt*on*$O(N_2O_2)$, we find that the N–O overlap population varies from 0.88 to 0.82 and, correspondingly, a strong N–N bond is formed (0.74). This overlap population is intermediate between that of dinitrogen dioxide **5** (0.61) and that of hyponitrite **8** (0.80). Clearly, there are other situations, especially with rhodium-based catalysts, where the coupled product may have significant N–N double bond character.

### Other Adsorption Geometries of $N_2O_2$

For other adsorption geometries of NO, coupling can lead to *on-top* $M(N_2O_2)$ **7b** and *perp* $M(N_2O_2)$ **7c**. The results for these adsorption geometries of $N_2O_2$ are very similar to those presented for *bridging* $M(N_2O_2)$ **7a**.

We need not discuss the reaction enthalpies in either geometry as the systems are much less stable. The differences in energy between *bridging* $M(N_2O_2)$ **7a** and either *on-top* $M(N_2O_2)$ **7b** and *perp* $M(N_2O_2)$ **7c** favor **7a** by at least 1.5 eV.

### Conclusion

The present study has focused on adhesive as well as catalytic properties of rhodium, palladium, and platinum on $\alpha$-$Al_2O_3$. The trends noted for the variation of the Fermi level as a function of metal–ceramic interface indicate that the ceramic may be more than an inert support.[79] Aluminum–metal and oxygen–metal interfaces are predicted to be stable for both palladium or platinum. The oxygen–metal interface, unstable for rhodium, is predicted to be particularly favorable both for dissociative adsorption of NO as well as for a coupling reaction, yielding a reduced form of $N_2O_2$.

With this study, we hope encourage experimentalists to design catalytic systems with well-defined interfaces to test our conclusions. Eventually, other ceramics with less electronegative elements could be tested, as a higher Fermi level for the ceramic should be reflected in the Fermi level of the resulting catalysts. We are currently testing these ideas.

**Acknowledgment.** Our research was supported by a grant from the Ford Motor Corp. T.R.W. is thankful to the Swiss National Science Foundation for the award of a postdoctoral fellowship. The stay of P.A. at Cornell University has been made possible through a postdoctoral grant of the *Ministerio de Educación y Ciencia* of Spain. We thank Dr. Mordecai Shelef and Dr. Ken Hass for many discussions and are grateful to Jane Jorgenson for her expert drawings.

### Appendix

Tight-binding extended Hückel calculations, with a weighted $H_{ij}$ approximation, have been applied throughout this paper. All $H_{ii}$'s were obtained from earlier work.[78,80] Extended Hückel parameters for all atoms used are listed in Table III.

**TABLE III: Extended Hückel Parameters**

| atom | orbital | $H_{ii}$ (eV) | $\xi_1$ | $\xi_2$ | $c_1$ | $c_2$ |
|---|---|---|---|---|---|---|
| H | 1s | −13.60 | 1.30 | | | |
| Al | 3s | −12.30 | 1.17 | | | |
| | 3p | −6.50 | 1.17 | | | |
| N | 2s | −23.95 | 1.95 | | | |
| | 2p | −10.95 | 1.95 | | | |
| O | 2s | −27.61 | 2.28 | | | |
| | 2p | −11.01 | 2.28 | | | |
| Rh | 5s | −7.31 | 2.13 | | | |
| | 5p | −3.39 | 2.10 | | | |
| | 4d | −10.35 | 4.29 | 1.97 | 0.5807 | 0.5685 |
| Pd | 5s | −7.24 | 2.19 | | | |
| | 5p | −3.68 | 2.15 | | | |
| | 4d | −11.90 | 5.98 | 2.61 | 0.55 | 0.67 |
| Pt | 6s | −9.15 | 2.55 | | | |
| | 6p | −4.38 | 2.55 | | | |
| | 5d | −11.00 | 6.01 | 2.70 | 0.63 | 0.55 |

Throughout this paper we used M–N 1.80 Å and N–O 1.17 Å. The three-layer two-dimensional slab of the fcc metal structures used nearest neighbor separations of 2.70 Å for all metal slabs.

The $k$ points were generated according to the geometrical method of Böhm and Ramirez.[81]

### References and Notes

(1) Farrauto, R. J.; Heck, R. M.; Speronello, B. K. *Chem. Eng. News* **1992**, *Sept 7*, 34.
(2) Taylor, K. C. *Chemtech* **1990**, *20*, 551.
(3) Pirug, G.; Bonzel, H. P.; Hopster, H.; Ibach, H. *J. Chem. Phys.* **1979**, *71*, 593.
(4) Carley, A. F.; Rassias, S.; Roberts, M. W.; Wang, T.-H. *Surf. Sci.* **1979**, *84*, L227.
(5) Schwartz, S. C.; Fisher, G. B.; Schmidt, L. D. *J. Phys. Chem.* **1988**, *92*, 389.
(6) Bowker, M.; Guo, Q.; Joyner, R. W. *Surf. Sci.* **1991**, *257*, 33.
(7) Brodén, G.; Rhodin, T. N.; Bruckner, C.; Benbow, R.; Hurych, Z. *Surf. Sci.* **1976**, *59*, 593.
(8) Bonzel, H. P.; Pirug, G. *Surf. Sci.* **1977**, *62*, 45.
(9) Klein, R. L.; Schwarz, S. C.; Schmidt, L. D. *J. Phys. Chem.* **1985**, *89*, 4908.
(10) Gorte, R. J.; Schmidt, L. D. *Surf. Sci.* **1981**, *111*, 260.
(11) Obuchi, A.; Naito, S.; Onishi, T.; Tamaru, K. *Surf. Sci.* **1982**, *122*, 235.
(12) Jorgenson, S. W.; Canning, N. D. S.; Madix, R. J. *Surf. Sci.* **1987**, *179*, 322.
(13) Conrad, H.; Ertl, G.; Küppers, J.; Latta, E. E. *Surf. Sci.* **1977**, *65*, 235.
(14) Ward, T. R.; Hoffmann, R.; Shelef, M. *Surf. Sci.*, submitted.
(15) Pashutski, A.; Folman, M. *Surf. Sci.* **1989**, *216*, 395.
(16) Ekwelundu, E. C.; Ignatiev, A. *Surf. Sci.* **1989**, *215*, 91.
(17) Kiota, T.; Kawana, A.; Miki, H.; Sugai, S.; Kawasaki, K. *Surf. Sci.* **1987**, *182*, 28.
(18) Tatarenko, S.; Alnot, M.; Ducros, R. *Surf. Sci.* **1985**, *163*, 249.
(19) Rodriguez, S. *Surf. Sci.* **1990**, *226*, 101.
(20) Tenner, M. G.; Kuipers, E. W.; Langhout, W. Y.; Kleyn, A. W.; Nicolasen, G.; Stolte, S. *Surf. Sci.* **1990**, *236*, 151.
(21) Kiota, T. *Surf. Sci.* **1989**, *222*, 140.
(22) Bartram, M. E.; Koel, B. E.; Carter, E. A. *Surf. Sci.* **1989**, *219*, 467.
(23) Gland, J. L.; Sexton, B. A. *Surf. Sci.* **1980**, *94*, 355.
(24) Hayden, B. E. *Surf. Sci.* **1983**, *131*, 419.
(25) Ormerod, R. M.; Lambert, R. M. *Surf. Sci.* **1990**, *225*, L 20.
(26) Schmick, H.-D.; Wassmuth, H.-W. *Surf. Sci.* **1982**, *123*, 471.
(27) Bertolo, M.; Jacobi, K. *Surf. Sci.* **1990**, *236*, 143.
(28) Yamada, T.; Matsuo, I.; Nakamura, J.; Xie, M.; Hirano, H.; Matsumoto, Y.; Tanaka, K.-I. *Sur. Sci.* **1990**, *231*, 304.
(29) Villarubia, J. S.; Ho, W. *J. Chem. Phys.* **1987**, *87*, 750.
(30) Dubois, L. H.; Hansma, P. K.; Somorjai, G. A. *J. Catal.* **1980**, *65*, 318.
(31) Richter-Addo, G. B.; Legzdins, P. *Metal Nitrosyls*; Oxford University Press: New York, 1992.
(32) deLouise, L. A.; Winograd, N. *Surf. Sci.* **1985**, *154*, 79.
(33) Hoffmann, R.; Chen, M. M.-L.; Elian, M.; Rossi, A. R.; Mingos, D. M. P. *Inorg. Chem.* **1974**, *13*, 2666–2675.
(34) Eisenberg, R.; Meyer, C. D. *Acc. Chem. Res.* **1975**, *8*, 26.
(35) Enemark, J. H.; Feltham, R. D. *Coord. Chem. Rev.* **1974**, *13*, 339.
(36) Hoffmann, R.; Chen, M. M.-L.; Thorn, D. L. *Inorg. Chem.* **1977**, *16*, 503.
(37) Nyberg, C.; Uvdal, P. *Surf. Sci.* **1988**, *204*, 517.
(38) Ibach, H.; Lehwald, S. *Surf. Sci.* **1978**, *76*, 1.
(39) Ghiotti, G.; Garrone, E.; Gatta, G. D.; Fubini, B.; Giamello, E. *J. Catal.* **1983**, *80*, 249.

(40) Garrone, E.; Ghiotti, G.; Giamello, E.; Fubini, B. *J. Chem. Soc., Faraday Trans. 1* **1981**, *77*, 2613.
(41) Zecchina, A.; Garrone, E.; Monterra, C.; Coluccia, S. *J. Phys. Chem.* **1975**, *79*, 978.
(42) Garrone, E.; Ghiotti, G.; Coluccia, S.; Zecchina, A. *J. Phys. Chem.* **1975**, *79*, 984.
(43) Morrow, B. A.; Sont, W. N.; Onge, A. S. *J. Catal.* **1980**, *62*, 304.
(44) Morrow, B. A.; Moran, L. E. *J. Catal.* **1980**, *62*, 294.
(45) Anderson, J. A.; Millar, G. J.; Rochester, C. H. *J. Chem. Soc., Faraday Trans.* **1990**, *86*, 571.
(46) Liang, J.; Wand, H. P.; Spicer, L. D. *J. Phys. Chem.* **1985**, *89*, 5840.
(47) Kazusaka, A.; Howe, R. F. *J. Catal.* **1980**, *63*, 447.
(48) Mauge, F.; Valet, A.; Bachelier, J.; Duchet, J. C.; Lavalley, J. C. *Catal. Lett.* **1989**, *2*, 57.
(49) Roustan, J. L.; Lijour, Y.; Morrow, B. A. *Inorg. Chem.* **1987**, *26*, 2509.
(50) Pearce, J. R.; Sherwood, D. E.; Hall, M. B.; Lunsford, J. H. *J. Phys. Chem.* **1980**, *84*, 3215.
(51) Newcomb, T. J.; Gopal, P. G.; Watters, K. L. *Inorg. Chem.* **1987**, *26*, 809.
(52) Morrow, B. A.; Baraton, M. I.; Lijour, Y.; Roustan, J. L. *Spectrochim. Acta* **1987**, *43A*, 1583.
(53) Marrow, B. A.; Baraton, M. I.; Roustan, J. L. *J. Am. Chem. Soc.* **1987**, *109*, 7541.
(54) Iizuka, T.; Lunsford, J. H. *J. Mol. Catal.* **1980**, *8*, 391.
(55) Praliaud, H.; Coudurier, G. F.; Taarit, Y. B. *J. Chem. Soc., Faraday Trans. 1* **1978**, *74*, 3000.
(56) Spoto, G.; Bordiga, S.; Scarano, D.; Zecchina, A. *Catal. Lett.* **1992**, *13*, 39.
(57) Bodenstein, M. *Helv. Chim. Acta* **1935**, *18*, 745.
(58) Greenwood, N. N.; Earnshaw, A. *Chemistry of the Elements*; Pergamon Press: Oxford, 1984.
(59) Rühle, M.; Evans, A. G. *Mater. Sci. Eng.* **1989**, *A107*, 187.
(60) Loehman, R. E. *Am. Ceram. Soc. Bull.* **1989**, *68*, 891.
(61) Alemany, P.; Boorse, R. S.; Burlich, J. M.; Hoffmann, R. *J. Phys. Chem.*, submitted.
(62) Alemany, P.; Boorse, R. S.; Burlich, J. M.; Hoffmann, R. *Chem. Mater.* **1993**, *5*, 465.
(63) Boorse, R. S.; Alemany, P.; Burlich, J. M.; Hoffmann, R. *Chem. Mater.* **1993**, *5*, 459.
(64) Kummer, J. T. *Prog. Energy Combust. Sci.* **1980**, *6*, 177.
(65) Ealet, B.; Gillet, E. *Surf. Sci.* **1993**, *281*, 91.
(66) Hoffmann, R.; Lipscomb, W. N. *J. Chem. Phys.* **1962**, *37*, 2872; **1962**, *36*, 2179. Hoffmann, R. *J. Chem. Phys.* **1963**, *39*, 1397.
(67) Whangbo, M.-H.; Hoffmann, R. *J. Am. Chem. Soc.* **1978**, *100*, 6093.
(68) Whangbo, M.-H.; Hoffmann, R.; Woodward, R. B. *Proc. R. Soc. London* **1979**, *A366*, 23.
(69) Donohue, J. *The Structure of the Elements*; Krieger, R. E., Publ. Comp., Inc: Malabar, FL, 1982.
(70) The consequences of making this approximation were tested by calculating a Pt slab with Rh and Pt cell parameters. The changes in Fermi level and total energy were small, and the DOS nearly identical.
(71) Wells, A. F. *Structural Inorganic Chemistry*; Clarendon Press: Oxford, 1990.
(72) Yao, Y. F.; Kummer, J. T. *J. Catal.* **1977**, *46*, 388.
(73) Yao, H.; Stephen, H.; Gandhi, H. *J. Catal.* **1980**, *61*, 547.
(74) Summers, J.; Ausen, S. *J. Catal.* **1979**, *58*, 131.
(75) Blyholder, G. *J. Phys. Chem.* **1964**, *68*, 2772.
(76) Hoffmann, R. *Solids and Surfaces: A Chemist's View of Bonding in Extended Structures*; VCH Publisher, Inc.: New York, Weinheim, 1988.
(77) Sung, S.-S.; Hoffmann, R.; Thiel, P. A. *J. Phys. Chem.* **1986**, *90*, 1380.
(78) Vučković, D. L.; Jansen, S. A.; Hoffmann, R. *Langmuir* **1990**, *6*, 732–746.
(79) Wey, J. P.; Neely, W. W. C.; Worley, S. D. *J. Phys. Chem.* **1992**, *96*, 7088.
(80) Wong, Y.-T.; Hoffmann, R. *J. Phys. Chem.* **1991**, *95*, 859–867.
(81) Ramirez, R.; Böhm, M. C. *Int. Quantum Chem.* **1986**, *30*, 391.